Journal of the Optical Society of America B
OPTICAL PHYSICS

Frequency generation in moving photonic crystals

Hang Qu,[1] Zoé-Lise Deck-Léger,[2] Christophe Caloz,[2] and Maksim Skorobogatiy[1,*]

[1]Engineering Physics, École Polytechnique de Montréal, Montréal, Québec H3C 3A7, Canada
[2]Electrical Engineering, École Polytechnique de Montréal, Montréal, Québec H3C 3A7, Canada
*Corresponding author: maksim.skorobogatiy@polymtl.ca

Received 21 March 2016; revised 30 May 2016; accepted 31 May 2016; posted 24 June 2016 (Doc. ID 261432); published 12 July 2016

In this paper, we discuss experimental feasibility and present several system designs that could be potentially used for generation of new frequencies by light waves interacting with moving photonic crystals. In particular, we first theoretically analyze multiple frequency generation when incident light is reflected or diffracted by the moving infinite 1D photonic crystals of different orientations. We then demonstrate frequency harmonics generation via leaky waves of a moving finite-size 1D photonic crystal. Finally, we study dispersion relations of modes guided in the hollow core of a moving waveguide. In particular, we demonstrate frequency comb generation inside of the hollow core of a moving 2D photonic crystal waveguide.

OCIS codes: (050.5298) Photonic crystals; (130.5296) Photonic crystal waveguides.

http://dx.doi.org/10.1364/JOSAB.33.001616

1. INTRODUCTION

In photonic crystals (PCs), dielectric constant exhibits periodic variation in one, two, or in all three orthogonal directions. Over the past 20 years, PCs became a very popular research topic, since such periodic structures could significantly influence the flow of light, and they were demonstrated to possess many unique optical properties. PCs find their uses in many practical fields, including optics [1–3], medicine [4,5], biology [6,7], telecommunications [8], fashion industry [9,10], among others. Most of the existing research, however, focused on the stationary PCs, while moving PCs were somewhat overlooked. Due to the relativistic effects, the interaction between light and a moving photonic crystal can lead to many intriguing phenomena akin to nonlinear effects in a stationary media. For example, we considered oscillating PCs in [11,12]. There, it was established that when the light of frequency ω_0 is incident onto a PC oscillating with frequency Ω, a frequency comb centered around ω_0 with a comb spacing Ω is generated. Notably, frequency combs are currently realized using nonlinear optical processes and high-power light sources [13,14], while moving PCs can achieve similar results using purely linear media. Moreover, a moving PC with a negative effective refractive index could induce an inverse Doppler effect, which was theoretically predicted by Veselago [15]. Recently, Chen *et al.* experimentally demonstrated this phenomenon at optical frequencies using a moving 2D PC prism [16]. Reed *et al.* considered a relative movement between a PC and a point light source by displacing an oscillating dipole inside a PC and observed the inverse Doppler effect [17,18]. Wang *et al.* emulated a "moving" PC by displacing a periodically modulated intensity of a standing wave generated by the two detuned counterpropagating waves inside of the electromagnetically induced transparency medium. Due to the relativistic Doppler effect, the PC exhibited different bandgaps for the light wave passing PC from the two opposite directions. Based on this phenomenon, they developed an optical isolator based on a moving PC [19]. The goal of this paper is to discuss major obstacles as well as possible system design solutions on the road of experimental realization of systems that utilize moving periodic media.

2. EXPERIMENTAL CHALLENGES AND SYSTEM DESIGN CONSIDERATIONS

While a number of intriguing theoretical propositions have been made about the use of moving PCs, their experimental demonstrations remain scarce. In part, this is due to the complexity of generation as well as detection of light in such systems. In particular, due to the relativistic nature of the Doppler effect, the generated harmonics and/or their amplitudes are proportional to the ratio of the PC characteristic velocity to the speed of light $\frac{v}{c}$. When using physical displacement, it is reasonable to assume that PC velocity under normal laboratory conditions will be limited to several kilometers/second. This can be realized either by directly mounting a PC onto a projectile, or placing it onto a rotating stage. Therefore, when using direct displacement of a PC, one expects $\frac{v}{c} \leq \frac{0.3\text{–}3\ \text{km/s}}{3\cdot10^5\ \text{km/s}} \sim 10^{-6}\text{–}10^{-5}$. As an example, if the fundamental bandgap wavelength of a PC is $\lambda_0 \approx 1\ \mu\text{m}$, a moving PC will generate harmonics with characteristic spacing

$\delta\lambda \sim \lambda_0 \cdot \frac{v}{c} \approx 1$–$10$ pm. Therefore, one has to use spectrometric methods capable of such a resolution to detect the effect of a moving PC on the flow of light. While in the visible spectral range, ∼1 pm resolution is somewhat challenging but certainly not impossible, an additional complication is caused by the short acquisition time due to the fast moving nature of a target. In this respect, mounting a PC onto a rotating stage that could provide significant linear velocity (≥300 m/s) is probably the most promising direct experimental approach as relatively high $\frac{v}{c} \sim 10^{-6}$ can be realized together with a possibility of using the lock-in acquisition technique due to the repetitive nature of a signal from a rotating PC.

Alternatively, stationary PCs can be realized via creation of periodic patterns in the photosensitive media by using optical standing waves of the same frequency Ω, or by using acoustic standing waves in the photoelastic media. Using slight detuning of frequencies ($\frac{\delta\Omega}{\Omega} \ll 1$) of the two waves forming standing waves, one can realize dynamic periodic patterns that can travel with significant velocities $\sim \frac{\delta\Omega}{\Omega} c$, where c is the speed of light in the photosensitive media, or a speed of sound in the photoelastic media. In both cases, velocities of the dynamically generated PCs can significantly surpass velocities of the mechanically displaced PCs. A drawback of these methods, however, is the relatively low refractive index contrast that can be generated in the photosensitive or photoelastic materials. In this case, a large number of periods should be used in order to profit from the bandgap effects, thus resulting in large PC samples. This might create its own experimental challenges related to the material uniformity across the sample, as well as the necessity of careful management of the experimental conditions at the sample boundaries. Notwithstanding of those challenges, several propositions have been made for the experimental realization of dynamic periodic systems, notably [19].

Finally, another important complication in the experimental realization of frequency generation in moving PCs is a simple fact that a detector has to be placed outside of the body of a moving PC. While a majority of papers on moving PCs discuss what happens inside of a moving PC, in this paper, we rather concentrate on various experimental scenarios of detection of radiation emitted by the moving PCs, while using a detector placed either completely outside of a PC or inside of a PC cavity such as a hollow core of a PC-based waveguide. We hope that our work could inspire future experimental research into moving PCs and their applications.

3. PLANE WAVE INCIDENT ONTO A SINGLE MOVING INTERFACE

We start by introducing Doppler frequency shift, when light is reflected by a moving planar interface between the free space and a dielectric. Consider two reference frames—a stationary frame S with coordinates (x, y, z, t) and a moving frame S' with coordinates (x', y', z', t'). The corresponding axes of the two frames are mutually parallel, and the frame S' moves at a constant velocity $\boldsymbol{v}$ with respect to the frame S along its x-axis. The spacetime in the frame S' could be related to the space time in the frame S via Lorentz transformation (LT),

$$\text{LT:}\quad \begin{aligned} t' &= \gamma\left(t - \tfrac{vx}{c^2}\right),\\ x' &= \gamma(x - vt),\\ y' &= y,\\ z' &= z, \end{aligned} \tag{1}$$

where c is the velocity of light in the free space, and $\gamma = \frac{1}{\sqrt{1-v^2/c^2}}$. The inverse Lorentz transformation (ILT) is then

$$\text{ILT:}\quad \begin{aligned} t &= \gamma\left(t' + \tfrac{vx'}{c^2}\right),\\ x &= \gamma(x' + vt'),\\ y &= y',\\ z &= z'. \end{aligned} \tag{2}$$

We also note that Maxwell's field equations are invariant under Lorentz transformation. Namely, according to [20], Maxwell's field equations in free space in the moving frame S' and in the stationary frame S are expressed as follows:

$$S'\text{:}\ \begin{aligned} \nabla' \cdot \boldsymbol{E}' &= 0,\\ \nabla' \times \boldsymbol{E}' &= -\tfrac{\partial \boldsymbol{B}'}{\partial t'},\\ \nabla' \cdot \boldsymbol{B}' &= 0,\\ \nabla' \times \boldsymbol{B}' &= \tfrac{\partial \boldsymbol{E}'}{c^2 \partial t'}, \end{aligned} \qquad S\text{:}\ \begin{aligned} \nabla \cdot \boldsymbol{E} &= 0,\\ \nabla \times \boldsymbol{E} &= -\tfrac{\partial \boldsymbol{B}}{\partial t},\\ \nabla \cdot \boldsymbol{B} &= 0,\\ \nabla \times \boldsymbol{B} &= \tfrac{\partial \boldsymbol{E}}{c^2 \partial t}, \end{aligned} \tag{3}$$

where $\boldsymbol{E}'$ and $\boldsymbol{B}'$ are the electric and magnetic fields in the frame S', and $\boldsymbol{E}$ and $\boldsymbol{B}$ are the electric and magnetic fields in the frame S, while assuming that charge and current densities are 0. The invariance of the Maxwell field equations under Lorentz transformation constitutes the basis for the following discussion. Thus, according to [20], the electric and magnetic fields in the free space in the two reference frames are related as follows:

$$\begin{aligned} \boldsymbol{E}' &= \gamma\boldsymbol{E} + (1-\gamma)\cdot(\boldsymbol{E}\cdot\boldsymbol{v})\frac{\boldsymbol{v}}{v^2} + \gamma(\boldsymbol{v}\times\boldsymbol{B}),\\ \boldsymbol{B}' &= \gamma\boldsymbol{B} + (1-\gamma)\cdot(\boldsymbol{B}\cdot\boldsymbol{v})\frac{\boldsymbol{v}}{v^2} - \frac{\gamma(\boldsymbol{v}\times\boldsymbol{E})}{c^2}, \end{aligned} \tag{4}$$

where $v = |\boldsymbol{v}|$. Equation (4) gives the fields in the frame S' in terms of the fields in the frame S. Equations giving the fields in the frame S in terms of the fields in the frame S' can be obtained by interchanging primed and unprimed quantities and replacing $\boldsymbol{v}$ by $\boldsymbol{v}'$, which is the velocity of the frame S relative to the frame S' as measured in the frame S'.

In the frame S, an electromagnetic plane wave with the angular frequency ω is incident along the $-x$ direction from the free space onto a moving medium with refractive index n_m. In what follows we assume that the refractive index of the free space is the same as that of air $n_{\text{air}} = 1$; therefore, we use the terms air and free space interchangeably. The air–dielectric interface M, while being orthogonal to the x-axis moves along the x-axis with a constant velocity $\boldsymbol{v}$ (Fig. 1). We define a wave vector $-\boldsymbol{k}$ with a negative sign to represent an incident plane wave, and assume that the electric field of the incident plane wave only has a z-component. Thus, we can write the electric field of the incident plane wave in the stationary frame S as

$$\boldsymbol{E}_I(x,t) = \hat{\boldsymbol{z}} \cdot E_Z^I e^{i(-kx-\omega t)}, \tag{5}$$

where E_z^I is the amplitude of the electric field. Note that the same plane wave in the moving frame S' could be expressed as

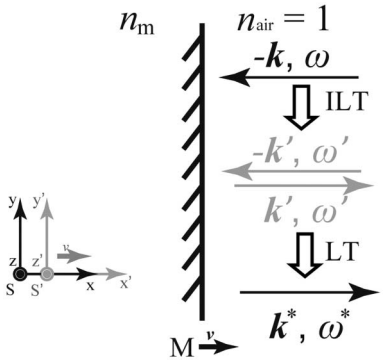

Fig. 1. Schematic of the reflection by a single moving interface. Using ILT, a plane wave defined by $(-\boldsymbol{k}, \omega)$ in the stationary frame S is converted into $(-\boldsymbol{k}', \omega')$ in the moving frame S' in which the reflected and transmitted waves can be easily described using basic optics. Then, the reflected and transmitted waves are transformed back into the stationary frame using LT.

$$\boldsymbol{E}_I'(x', t') = \hat{\boldsymbol{z}}' \cdot E_z^{I'} e^{i(-k'x' - \omega' t')}. \tag{6}$$

According to Eq. (4), in the case of plane waves, the amplitude of the electric field in the S' frame is related to the amplitude of the electric field in the S frame as (see Appendix A)

$$E_Z^{I'} = \gamma E_Z^I \left(1 - \frac{v}{c}\right). \tag{7}$$

In order to find $\boldsymbol{k}'$ and ω', we apply ILT (2) to the phase components in Eq. (5), and then compare the resultant phase components with their counterparts in Eq. (6). The relationship between $(\boldsymbol{k}, \omega)$ and $(\boldsymbol{k}', \omega')$ are then as follows:

$$\boldsymbol{k}' = \hat{\boldsymbol{x}}' \left(k\gamma + \frac{\omega v \gamma}{c^2}\right), \omega' = kv\gamma + \omega\gamma. \tag{8}$$

After substituting the plane wave dispersion relation $k = \omega/c$ into Eq. (8), we find

$$\omega' = \omega\gamma \left(1 + \frac{v}{c}\right), \boldsymbol{k}' = \boldsymbol{k}\gamma \left(1 + \frac{v}{c}\right). \tag{9}$$

Equation (9) indicates that the frequency of a plane wave in the frame S is changed by the factor $\gamma(1 + \frac{v}{c})$ when measured in the frame S'. This is a well-known relativistic Doppler effect. In the frame S', the interface M is stationary. Thus, the plane wave reflected by the interface M has the following electric field:

$$\boldsymbol{E}_R'(x', t') = \hat{\boldsymbol{z}}' \cdot r E_Z^{I'} e^{i(k'x' - \omega' t')}, \tag{10}$$

where $r = \frac{1 - n_m}{1 + n_m}$ is the Fresnel amplitude reflection coefficient. In order to find the electric field of the reflected wave in the stationary frame S, we now apply Lorentz transformation (1) to the phase components in Eq. (10) and find the form of the reflected plane wave in the frame S. In particular, the corresponding wave vector $\boldsymbol{k}^*$ and angular frequency ω^* of the reflected wave in the frame S are

$$\omega^* = \omega\gamma^2 \left(1 + \frac{v}{c}\right)^2,$$
$$\boldsymbol{k}^* = \boldsymbol{k}\gamma^2 \left(1 + \frac{v}{c}\right)^2. \tag{11}$$

If the velocity v is much smaller than the speed of light c in free space, the angular frequency ω^* could be approximated as

$$\omega^* \underset{v/c \ll 1}{\approx} \omega \left(1 + \frac{2v}{c}\right). \tag{12}$$

Equation (12) describes a classic Doppler frequency shift. Moreover, we can also find the amplitude of the reflected electromagnetic field in the stationary frame S by exchanging the primed and unprimed quantities in Eqs. (A1)–(A8). Thus, we find that the amplitude of the reflected electric field is related to the amplitude of the incident electric field as

$$|\boldsymbol{E}_R^*| = |\boldsymbol{E}_R'| \left(1 - \frac{v}{c}\right)\gamma = r\gamma^2 \left(1 - \frac{v}{c}\right)^2 E_Z^I$$
$$= rE_Z^I \left(1 - \frac{v}{c}\right) / \left(1 + \frac{v}{c}\right) \underset{v/c \ll 1}{\approx} rE_Z^I \left(1 - 2\frac{v}{c}\right). \tag{13}$$

4. PLANE WAVE INCIDENT ONTO A MOVING PC

So far, we have discussed interaction of a plane wave with a moving planar interface. The wave vector and frequency of the incoming light are first found in the moving reference frame in which the interface is stationary. The reflected (or diffracted) wave in the moving frame could then be easily found using standard optics considerations. Then, the form of a reflected wave in the stationary frame is found by transformation from the moving frame S' back into the fixed frame S. Following the same methodology, in what follows, we consider interaction of a plane wave with one- or two-dimensional PCs that move along the x-axis with a velocity $\boldsymbol{v}$. We use the same strategy to find the frequency of the reflected or diffracted light as in the case of a single interface by first solving the problem in the moving reference frame where the PC is stationary and then transforming thus found solution into the stationary reference frame.

A. Moving 1D PC

We first discuss reflection by a moving 1D PC consisting of a dielectric multilayer with alternating high- and low-refractive indices. The dielectric constant of a 1D PC is a periodic function along the x-axis, and it is homogeneous in the YOZ plane (Fig. 2). In the frame S', when the plane wave with a wave vector $-\boldsymbol{k}'$ is incident normally onto the multilayer, no harmonics are generated in the reflection as only a single reflected wave is generated with a wave vector $\boldsymbol{k}'$. Consequently, when converted back into the stationary frame S, the corresponding wave vector $\boldsymbol{k}^*$ and frequency ω^* would be identical to those presented in Eq. (11), thus predicting a standard Doppler shift for the plane wave reflected from a moving PC.

B. Moving 1D PC (Transverse Orientation)

In general, a reflective diffraction grating consists of a spatially periodic arrangement of groves inscribed onto a planar substrate. When a plane wave is incident normally onto a

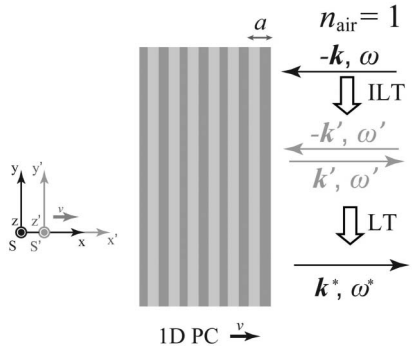

Fig. 2. Schematic of reflection by a semi-infinite moving 1D PC.

diffraction grating or a 1D PC in the transverse orientation, it will be diffracted. A well-known grating equation [Eq. (14)] is used to describe the dependence of the diffraction angle θ' (with respect to the x-axis) in the moving frame S' on the wavelength λ' of the normally incident plane wave, the grating pitch a, and the diffraction order m [21]:

$$a \cdot \sin \theta'_m = m\lambda'. \tag{14}$$

A schematic of diffraction from a moving diffraction grating or a 1D PC is shown in Fig. 3. Following the same procedure as in Section 3, the wave vector $-\boldsymbol{k}$ and angular frequency ω of the plane wave in the stationary frame are converted into $-\boldsymbol{k}'$ and ω' in the moving frame. The wave vector of diffracted waves could then be decomposed into x' and y' components and then transformed back into the stationary frame. Practically, assuming that the electric field of the normally incident plane wave is directed along the z-axis we write

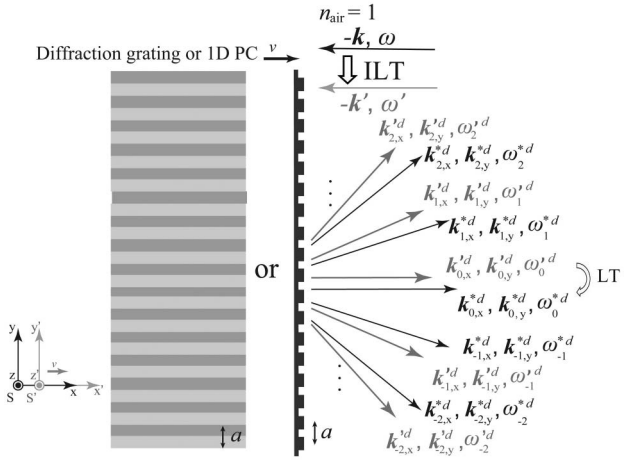

Fig. 3. Schematic of diffraction by the moving reflective diffraction grating or a 1D PC in the transverse orientation. $(k'^d_{m,y}, k'^d_{m,x})$ and $(k^{*d}_{m,y}, k^{*d}_{m,x})$ are calculated using Eqs. (16) and (17) assuming that the period a of the diffraction grating or a 1D PC is 3 μm, and frequency of the incident plane wave is $\omega = 2\pi c/\lambda_0$, $\lambda_0 = 1$ μm, while $v/c = 0.1$. Here, we chose $v/c = 0.1$ so that in Fig. 3, the propagation directions of the diffracted wave vectors $(k^{*d}_{m,y}, k^{*d}_{m,x})$ in the stationary reference frame S could be visually distinguished from those of the wave vectors $(k'^d_{m,y}, k'^d_{m,x})$ in the moving frame S'.

$$\boldsymbol{E}'_{d,m}(x', y', t') = \hat{\boldsymbol{z}}' \cdot E'_{d,m} \cdot e^{i(k'^d_{m,x}x' + k'^d_{m,y}y' - \omega' t')},$$
$$k'^d_{m,x} = k' \cos \theta'_m,$$
$$k'^d_{m,y} = k' \sin \theta'_m. \tag{15}$$

Combining Eq. (15) with Eq. (14), we find

$$k'^d_{m,y} = \frac{2\pi m}{a},$$
$$k'^d_{m,x} = \sqrt{\left(\frac{\omega'}{c}\right)^2 - \left(\frac{2\pi m}{a}\right)^2}. \tag{16}$$

Substituting Eq. (16) into Eq. (15), and then applying the Lorentz transformation to the phase components of the resultant expression, we could find the wave vector and angular frequency of the diffracted waves in the stationary frame S as follows:

$$k^{*d}_{m,y} = \frac{2\pi m}{a},$$
$$k^{*d}_{m,x} = \gamma\left(\sqrt{\left(\frac{\omega'}{c}\right)^2 - \left(\frac{2\pi m}{a}\right)^2} + \frac{\omega' v}{c^2}\right),$$
$$\omega^{*d}_m = \gamma\omega' + \frac{v\gamma}{c}\sqrt{(\omega')^2 - \left(\frac{2\pi mc}{a}\right)^2},$$
$$\omega' = \omega\gamma\left(1 + \frac{v}{c}\right). \tag{17}$$

Note that for the zeroth-order diffraction ($m = 0$), the frequency of the diffracted wave is identical to that reflected by a moving planar interface $\omega\gamma^2(1 + \frac{v}{c})^2$. For other higher-order diffracted waves, the corresponding angular frequencies ω^{*d}_m $(m > 0)$ would be confined between $\omega\gamma^2(1 + \frac{v}{c})$ and $\omega\gamma^2(1 + \frac{v}{c})^2$. Finally, we note that waves of different orders diffracted by the moving grating have frequencies and directions that are only slightly $(\sim \frac{v}{c})$ different from those of the waves diffracted by a stationary grating [see Eq. (17)]. The same also holds for the field amplitudes of the diffracted waves, which are virtually the same as in the case of a stationary grating [see Eq. (13)].

C. Harmonics Generation via Leaky Waves of a Moving 1D PC

In Section 4.A, we discussed reflection of a plane wave from a semi-infinite moving 1D PC and concluded that only a standard Doppler frequency shift is observed in this case. We now demonstrate that generation of harmonics is, nevertheless, possible in a PC that is semi-infinite or finite in the y direction. Such harmonics can be detected in the free space outside of a PC using a stationary detector in the frame S (see Fig. 4). It is well known that for infinite 1D PCs there exist regions of frequency space called bandgaps, inside of which no delocalized electromagnetic waves are permitted to propagate in the bulk of a PC [1]. Within a bandgap, the modes of a 1D PC are evanescent, exhibiting exponential decay inside of a multilayer. Outside of the bandgaps, the electromagnetic waves propagating in the multilayer satisfies the Bloch theorem due to discrete translational symmetry in the x direction. In fact, even for the semi-infinite or finite-size photonic crystals (in the z

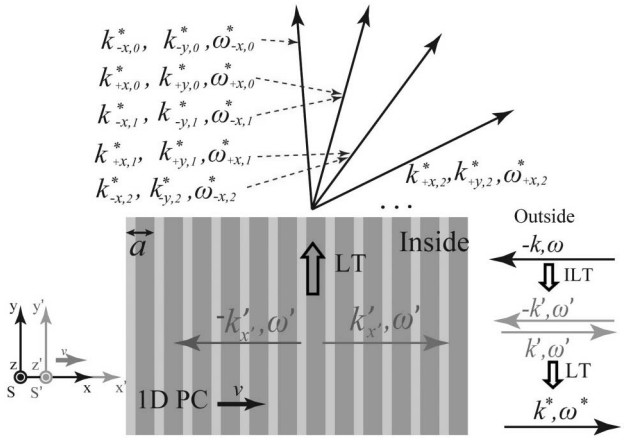

Fig. 4. Schematic of the leaky waves of a moving 1D PC. A 1D PC consists of the alternating high- and low-refractive index layers ($n_h = 4.5$, $n_l = 1.5$). The thicknesses of high- and low-refractive index layers are chosen to satisfy the quarter-wave conditions $d_{h,l} = \lambda_0/n_{h,l}$ at the wavelength λ_0 (see page 72 in [1]). $(k^*_{\pm x,n}, k^*_{\pm y,n}, \omega^*_{\pm,n})$ are calculated using Eqs. (24)–(27) assuming that the frequency of the incident plane wave (in the S' frame) corresponds to the lower edge of the seventh-order bandgap $\omega' \approx 13 \cdot 2\pi c/\lambda_0$, $k'_{x'} = \pi/a$, while $v/c = 0.1$. Note that in this case the vectors $(k^*_{+x,n-1}, k^*_{+x,n-1}, \omega^*_{+,n-1})$ overlap with the vectors $(k^*_{-x,n}, k^*_{-x,n}, \omega^*_{-,n})$.

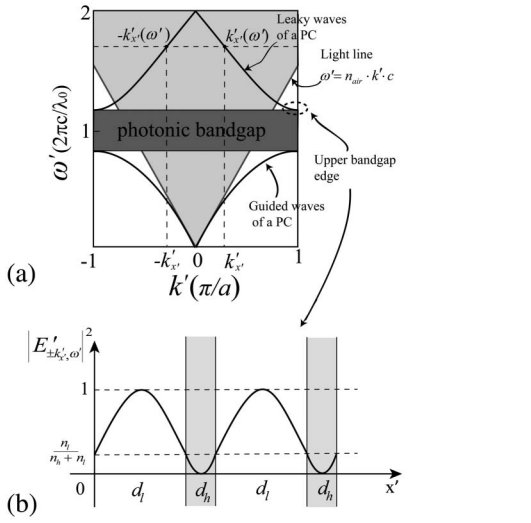

Fig. 5. (a) Dispersion relations of the guided waves propagating perpendicular to the periodic multilayer [1]. The light gray region defines a continuum of radiation states in the free space. Guided waves in the radiation continuum become leaky waves. The dark gray region defines the bandgap of the multilayer (see page 47 in [1]). (b) Field intensity at the upper edge of the first photonic bandgap (see Fig. 3.7 on page 77 in [1]).

and y direction), Bloch theorem still applies as long as there is a discrete translational symmetry in the x direction. Finally, even when a finite (in the x direction) PC is considered, modes inside of a finite PC can be developed in terms of a linear combination of the counterpropagating guided modes of an infinite (in the x direction) PC with expansion coefficients that are determined from the continuity of the transverse components of the electromagnetic fields on the PC boundaries with the free space.

In what follows, we assume that a plane wave incident onto a 1D PC has a frequency ω' (in the S' frame) located outside of the PC bandgaps. Also we assume that the electric field of an incident plane wave is directed along the z'-axis along which the 1D PC is assumed to be infinite. Moreover, the incoming plane wave is assumed to be normal to the 1D PC multilayer and it is characterized by a wave vector $-\boldsymbol{k}'$ directed along the x'-axis. The plane wave polarization is chosen so that only TE modes of a 1D PC are excited. If PC is finite in the x' direction, an incident plane wave with frequency ω' excites two counterpropagating modes of a 1D PC with wave vectors $k'_{x'}$ and $-k'_{x'}$ (see Fig. 5). The electric fields of the two TE modes of a PC could be expressed in the S' frame as follows [1]:

$$\boldsymbol{E}'_{\pm \mathrm{TE}}(x', y', t') = \hat{\boldsymbol{z}}' \cdot E'_{\pm k'_{x'},\omega'}(x', y') e^{i(\pm k'_{x'} x' - \omega' t')}, \qquad (18)$$

where according to the Bloch theorem, $E'_{\pm k'_{x'},\omega'}(x', y')$ are the periodic functions in the x' direction with a period a (the thickness of a bilayer in a PC multilayer). Note that $k'_{x'}$ in Eq. (18) is confined to the one-dimensional Brillouin zone $-\pi/a < k'_{x'} \le \pi/a$.

A typical band diagram of the modes of a finite (in the y direction) PC is presented in Fig. 5. In what follows, we assume that the PC size in the y' direction is much larger than its period and the wavelength of operation ($d \gg a, d \gg \lambda_0$). Under these assumptions, and considering that the PC is infinite in the z' direction, then its band diagram will look very similar to the one pertaining to an infinite (in the y' direction) PC. Here, we assume that only modes propagating along the x' direction are excited due to normal incidence angle of the incident plane wave. Such modes are characterized by the Bloch wave vectors $\pm k'_{x'}$, and their dispersion relations (solid lines in Fig. 5) are given by $\pm k'_{x'}(\omega')$. Due to the finite size of a PC in the y direction, the band diagram (as compared to that of a PC, which is infinite in the y' direction) has to be modified by including a continuum of states propagating in the free space. These states are plane waves propagating along all possible directions in the XOY plane. In this case, modes guided within a PC become phase matched with the modes of a radiation continuum and, therefore, become leaky modes. Thus, by choosing a high enough frequency of the excitation plane wave incident normally (along the x' direction) onto a moving PC, we can excite leaky guided modes inside of a PC, which can then leak out into free space sideways (along the y' direction). Such leaky waves can then be registered as harmonics by the stationary detector (in the S frame) outside of a moving PC.

Note that Eq. (18) holds both inside and outside of a PC. In what follows, we only consider Eq. (18) outside of a PC in the free space. There, applying LT to Eq. (18), we could transform the waveform back into the stationary frame S:

$$\text{Air: } \boldsymbol{E}^*_{\pm}(x, y, t) \propto \hat{\boldsymbol{z}} \cdot E'_{\pm k'_{x'},\omega'}(\gamma(x - vt), y) \times e^{i(\gamma(\pm k'_{x'} + \frac{\omega' v}{c^2})x - \gamma(\pm k'_{x'} v + \omega')t)}. \qquad (19)$$

Equation (19) constitutes the general form of a solution for the electric field of the TE modes outside of a 1D PC in the stationary S frame. Note that in Eq. (19) we do not show the

contributions of the $\boldsymbol{B}$ fields for the sake of simplicity. These terms [see Eqs. (4)] have the same dependence of the phase on x' and t', and they also feature a multiplier function that is periodic in the x' direction with a period a. Thus, omission of the terms containing $\boldsymbol{B}$ fields does not affect our further derivations for the frequencies and wave vectors of the side-emitted leaky waves.

Since $E'_{\pm k'_{x'},\omega'}(x',y')$ is a periodic function in the x' direction with a period a, it can be presented in terms of the discrete Fourier series,

$$E'_{\pm k'_{x'},\omega'}(x',y') = \sum_{n=-\infty}^{+\infty} A^n_{\pm k'_{x'},\omega'}(y') \cdot e^{i\frac{2\pi n}{a}x'}, \tag{20}$$

where n is an integer and $A^n_{\pm k'_{x'}}(y')$ are the Fourier coefficients that represent amplitude of the generated harmonics. To understand further dependence of the harmonic amplitudes on the harmonic order, we now evaluate Fourier coefficients associated with a periodic part of the field distribution in the leaky modes of a PC [Eq. (20)]. Modal distribution in the leaky modes of a PC in the vicinity of the upper edge [see Fig. 5(b)] will be similar to that of a mode at the upper bandgap edge ($k'_x = \pi/a$) for which analytical expression is known (see Fig 3.8 on page 77 in [1]). In particular, in the case of a high refractive index contrast ($n_h \gg n_l$), there would be virtually no field in the high refractive index layer with most of the field concentrated in the low refractive index layer, which could be approximated as

$$E'_{\pm k'_{x'},\omega'}(x',y') = \begin{cases} \sin\left(\frac{x'}{d_l}\cdot\pi\right), & x' \in [0, d_l] \\ 0, & x' \in [d_l, d_h] \end{cases}, \tag{21}$$

where the d_l and d_h are the thickness of the high- and low-refractive index layers, respectively, and $d_l + d_h = a$. Thus, the Fourier coefficients in Eq. (20) could be calculated as follows:

$$A^n_{\pm k'_{x'},\omega'}(y') = \frac{1}{a}\int_0^a E'_{\pm k'_{x'},\omega'}(x',y') \cdot e^{\frac{-i2\pi n x'}{a}} \mathrm{d}x'. \tag{22}$$

Equation (22) could be solved as

$$A^n_{\pm k'_{x'},\omega'}(y') = \frac{\pi}{a\mathrm{d}_l} \cdot \frac{e^{\frac{-i2\pi n}{a}\mathrm{d}_l} - 1}{(\frac{\pi}{d_l})^2 - (\frac{2\pi n}{a})^2}$$

$$\Rightarrow |A^n_{\pm k'_{x'},\omega'}(y')| = \frac{2a d_l}{\pi} \cdot \left| \frac{\sin(\frac{\pi n d_l}{a})}{a^2 - (2nd_l)^2} \right|. \tag{23}$$

From Eq. (23), we find that the amplitude of the generated harmonics is a sensitive function of the harmonic order number n, and for high-order numbers the harmonic amplitude decreases very fast as $|A^n_{\pm k'_{x'},\omega'}(y')| \propto n^{-2}$. From Eq. (22), we also conclude that the amplitude of a harmonic will be a sensitive function of the shape of the modal distribution. In the most extreme case, if the modal field is confined to the region of space of size d, which is much smaller than the PC period a, then electric field can be approximated as a delta function $\delta(x')$, which would result in constant amplitude for the generated harmonics up to the very high orders $n \sim a/d$. In passing we notice that this scenario is indeed possible in the case of weakly coupled photonic crystal resonator arrays, where the effective period (distance between resonators) can be made much larger than the resonator size, which defines modal field size in the resonance.

Finally, substituting Eq. (20) into Eq. (19), we finally get

$$\text{Air: } \boldsymbol{E}^*_{\pm}(x,y,t) \propto \hat{\boldsymbol{z}} \cdot \sum_{n=-\infty}^{+\infty} A^n_{\pm k'_{x'},\omega'}(y) e^{i(k^*_{\pm x,n}x - \omega^*_{\pm x,n}t)}, \tag{24}$$

where

$$k^*_{\pm x,n} = \pm k'_{x'}(\omega')\gamma + \frac{\omega' v\gamma}{c^2} + \frac{2\pi n\gamma}{a},$$

$$\omega^*_{\pm,n} = \omega'\gamma \pm k'_{x'}(\omega')v\gamma + \frac{2\pi v n\gamma}{a},$$

$$\omega' = \omega\gamma\left(1 + \frac{v}{c}\right). \tag{25}$$

Moreover, note that Eq. (24) is derived for the free space outside of a 1D PC. There, radiation can be expanded into TE-polarized plane waves $\propto e^{i(k^*_x x + k^*_y y - \omega t)}$ with the wave vector components satisfying a standard dispersion relation in the form $k^{*2}_x + k^{*2}_y = (\frac{\omega^*}{c})^2$. From this we conclude that $A^n_{\pm k'_{x'},\omega'}(y)$ in Eq. (24) should be necessarily in the form $A^n_{\pm k'_{x'},\omega'}(y) = A^n_{\pm k'_{x'},\omega'} e^{ik^*_{\pm y,n}y}$. Therefore, the electric field of the leaky PC mode in the free space can be presented as

$$\text{Air: } \boldsymbol{E}^*_{\pm}(x,y,t) \propto \hat{\boldsymbol{z}} \cdot \sum_{n=-\infty}^{+\infty} A^n_{\pm k'_{x'},\omega'} \cdot e^{i(k^*_{\pm x,n}x + k^*_{\pm y,n}y - \omega^*_{\pm,n}t)}, \tag{26}$$

where

$$k^*_{\pm y,n} = \sqrt{\left(\frac{\omega^*_{\pm,n}}{c}\right)^2 - (k^*_{\pm x,n})^2}$$

$$= \sqrt{\left(\frac{\omega'}{c}\right)^2 - \left(\frac{2\pi n}{a} \pm k'_{x'}(\omega')\right)^2}. \tag{27}$$

To summarize, Eqs. (24)–(27) indicate that upon launching a single-frequency plane wave normally onto a moving PC which is finite in the transverse direction, two types of frequency harmonics will be emitted sideways into the free space, which can then be registered using a stationary detector outside of a PC.

D. Moving Hollow-Core Bragg Waveguide

We now study guided modes of a moving hollow-core planar photonic bandgap Bragg waveguide. Such waveguides feature a hollow core sandwiched between two semi-infinite planar Bragg reflectors (Fig. 6). The reflector layers are parallel to the XOZ plane while the waveguide is directed along the x-axis. Moreover, Bragg waveguide moves with a constant velocity $\boldsymbol{v}$ along the x-axis in the frame S, while a stationary detector is located in the free space inside of the waveguide hollow core. We suppose that the waveguide has a finite length in the x direction, and therefore, an incident plane wave would generally excite two counterpropagating waves inside of the waveguide core. In the moving frame S', the waveguide is at rest, and the electric fields of its counterpropagating core guided modes can be written as follows [1]:

$$\boldsymbol{E}'_{\pm\beta'(\omega')}(x',y',t') = \boldsymbol{U}'_{\pm\beta'(\omega')}(y') e^{i[\pm\beta'(\omega')x' - \omega' t']}, \tag{28}$$

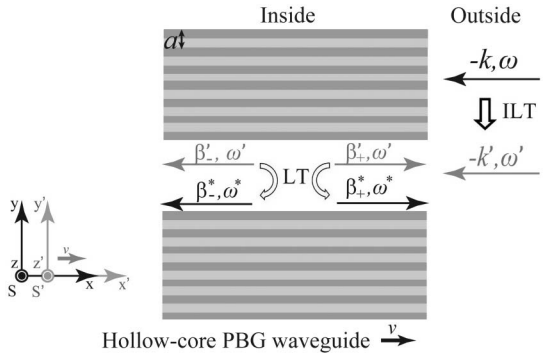

Fig. 6. Schematic of the excitation of guided modes in a semi-infinite moving hollow-core planar Bragg waveguide.

where $\boldsymbol{U}'_{\pm\beta'(\omega')}(y')$ is a vector function describing distribution of the modal electric field along the y' axis, β' is a modal propagation constant, while $\beta'(\omega')$ defines the modal dispersion relation (see Fig. 7).

Here, we consider the case of a single-mode Bragg waveguide shown in Fig. 7. In the case of a multimode Bragg waveguide, one has to consider all the excited guide modes, which results in the generation of multiple frequencies. Using LT we transform Eq. (28) back into the frame S:

$$\boldsymbol{E}^*_{\pm}(x,y,t) \propto \boldsymbol{U}'_{\pm\beta'(\omega')}(y)e^{i[\pm\beta'(\omega')\gamma(x-vt)-\omega'\gamma(t-\frac{v}{c^2}x)]}. \tag{29}$$

From Eq. (9), $\omega' = \omega\gamma(1+\frac{v}{c})$, while $\beta'(\omega')$ is the modal dispersion relation in the frame S' where the Bragg waveguide is stationary. By substituting ω' into Eq. (29), we could obtain the propagation constant β^* and frequency ω^* of the two counterpropagating modes of the hollow-core Bragg fiber in the stationary frame S:

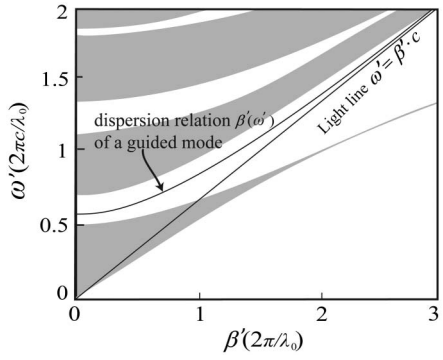

Fig. 7. Example of a band diagram of a periodic multilayer with a single layer defect. The 1D PC consists of the alternating high- and low-refractive index layers ($n_h = 2.8$, $n_l = 1.5$). The thickness of the multilayer materials is optimized for the light with a wavelength λ_0. In particular, the quarter-wave condition at the glancing incident angles is satisfied $d_{h,l} = \lambda_0/(4\sqrt{\epsilon_{h,l} - \epsilon_a})$. The core size is $d_c = 2d_l$. The solid thick line defines the dispersion relation of the fundamental bandgap core-guided mode. The gray regions represent continuum of the delocalized states in the multilayer (see page 85 in [1]).

$$\begin{aligned}\beta^*_{\pm} &= \pm\beta'(\omega')\gamma + \frac{\omega' v\gamma}{c^2},\\ \omega^*_{\pm} &= \omega'\gamma \pm \gamma\beta'(\omega')v,\\ \omega' &= \omega\gamma\left(1+\frac{v}{c}\right).\end{aligned} \tag{30}$$

We note that Eq. (30) defines the new dispersion relations of the guided modes in the moving hollow-core photonic bandgap (PBG) waveguide in the stationary frame S, while $\beta'(\omega')$ is the modal dispersion relation of a stationary waveguide in the moving frame S'. Note that expressions (30) are applicable to any hollow-core planar waveguide, and are not exclusive to the hollow-core Bragg waveguides.

As an example, consider the modes of a hollow-core planar metallic waveguide of a core size d_c. As is well known from the basic theory of waveguides, the dispersion relation of the core guided modes in such a waveguide is simply

$$\beta'(\omega') = \frac{1}{c}\sqrt{(\omega')^2 - (\omega^n_c)^2}, \tag{31}$$

or alternatively $(\omega')^2 = (c\beta'(\omega'))^2 + (\omega^n_c)^2$, where $\omega^n_c = \frac{\pi c n}{d_c}$, $(n \in N)$ is a cutoff frequency of the n_{th} guided mode of a hollow metallic waveguide. Then, according to Eqs. (30) and (31), dispersion relations of the counterpropagating modes of a moving hollow-core planar metallic waveguide will be

$$\begin{aligned}\beta^*_{\pm} &= \pm\frac{\gamma}{c}\sqrt{(\omega')^2 - (\omega^n_c)^2} + \frac{\omega' v\gamma}{c^2},\\ \omega^*_{\pm} &= \omega'\gamma \pm \frac{v\gamma}{c}\sqrt{(\omega')^2 - (\omega^n_c)^2},\\ \omega' &= \omega\gamma\left(1+\frac{v}{c}\right).\end{aligned} \tag{32}$$

Using Eq. (32), we plot in Fig. 8 the dispersion relation of a guided mode of a moving hollow-core planar metallic waveguide in the stationary frame S. As shown in Figs. 8(b) and 8(c), modal cutoff frequencies exhibit redshift from ω^n_c to $\omega^n_c/\gamma(1+\frac{v}{c})$. Note that in order to demonstrate a visually pronounced frequency shift in Fig. 8, we let $v/c = 0.1$.

From Eq. (32), we conclude that for a moving hollow-core waveguide, modal cutoff frequencies exhibit redshift from ω^n_c to $\omega^n_c/\gamma(1+\frac{v}{c})$. Moreover, in the vicinity of a new cutoff frequency $\omega = \omega^n_c/\gamma(1+\frac{v}{c})$, effective refractive indices of the guided modes as well as their group velocities can be expressed as follows:

$$\begin{aligned}&n^*_{\pm\text{eff}}\big|_{\omega=\frac{\omega^n_c}{\gamma(1+\frac{v}{c})}} = \frac{\beta^*_{\pm}c}{\omega^*_{\pm}} = \frac{v}{c}; \qquad v^*_{\pm g} = \left.\frac{\partial\omega^*_{\pm}}{\partial\beta^*_{\pm}}\right|_{\omega=\frac{\omega^n_c}{\gamma(1+\frac{v}{c})}} = v\\ &\omega^*_{\pm}\big|_{\omega=\frac{\omega^n_c}{\gamma(1+\frac{v}{c})}} = \gamma\omega^n_c; \qquad \beta^*_{\pm}\big|_{\omega=\frac{\omega^n_c}{\gamma(1+\frac{v}{c})}} = \frac{\omega^n_c v\gamma}{c^2},\end{aligned} \tag{33}$$

while the modal chromatic dispersion $\sim\partial^2\beta^*_-/\partial^2\omega^*_-$ changes sign at $\omega = \omega^n_c/(1+\frac{v}{c})$ for the β^*_- mode:

$$\begin{aligned}&n^*_{-\text{eff}}\big|_{\omega=\frac{\omega^n_c}{1+\frac{v}{c}}} = 0; \qquad v^*_{-g} = \left.\frac{\partial\omega^*}{\partial\beta^*}\right|_{\omega=\frac{\omega^n_c}{1+\frac{v}{c}}} = 0\\ &\omega^*_{-}\big|_{\omega=\frac{\omega^n_c}{1+\frac{v}{c}}} = \omega^n_c; \qquad \beta^*_{-}\big|_{\omega=\frac{\omega^n_c}{1+\frac{v}{c}}} = 0.\end{aligned} \tag{34}$$

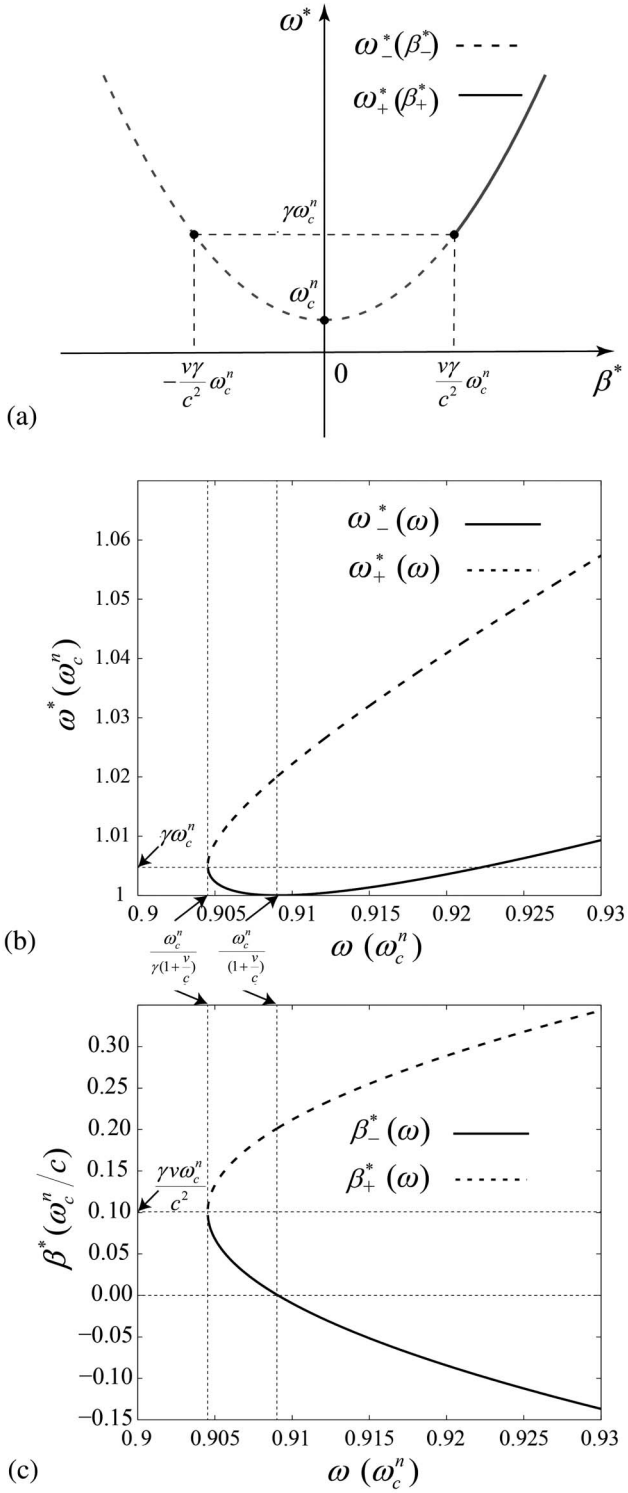

Fig. 8. (a) Dispersion relations of the two counterpropagating modes guided in a moving hollow-core metallic waveguide. (b)–(c) Same two dispersion relations, however, now as a function of the excitation frequency ω. Notice that in the frequency range $\omega \in [\omega_c^n/(1+\frac{v}{c})\gamma, \omega_c^n/(1+\frac{v}{c})]$ the signs of the $\beta^*_\pm$ propagation constants are both positive. Therefore, in this frequency range, both core guided modes can only propagate in the direction opposite to the direction of the incident light. This is only possible in the case of a short finite waveguide due to reflection from the waveguide outcoupling end. In the case of an infinite waveguide, effective cutoff frequency will, therefore, be $\omega_c^n/(1+\frac{v}{c})$.

Finally, we note from Eq. (32) that dispersion relations of the core guided modes of a moving hollow-core metallic waveguide satisfy the same simple dispersion relation as the modes of a stationary waveguide Eq. (31) $(\omega^*_\pm)^2 = (c\beta^*_\pm(\omega'))^2 + (\omega_c^n)^2$.

E. Moving Hollow-Core 2D PC Waveguide

Finally, we study frequency generation in the hollow core of a moving 2D hollow-core photonic crystal waveguide. In Fig. 9, we present an example of such a waveguide with a hollow core surrounded by a photonic crystal cladding featuring a square lattice of dielectric rods. The waveguide is homogeneous along the z' direction and periodic along the x' and y' directions with the lattice constant a. Waveguide hollow core is a defect introduced into the infinite photonic crystal by removing one row of the dielectric rods. The photonic crystal is moving along the x-axis at a constant velocity $\boldsymbol{v}$ in the frame S. In the frame S', the photonic crystal is stationary. For the sake of simplicity, we consider the TE-polarized mode of a waveguide excited by the incident plane wave polarized in the z direction. In the case of a finite size (in the x' direction) PC, when a plane wave with a wave vector $-\boldsymbol{k}'$ is incident onto a photonic crystal waveguide in the frame S', the plane wave excites two counterpropagating modes in the waveguide core that have the electric fields in the Bloch form (see page 150 in [1]):

$$\boldsymbol{E}'_\pm(x',y',z',t') = \hat{\boldsymbol{z}}' \cdot U'_{\pm\beta'(\omega')}(x',y')e^{i(\pm\beta'(\omega')x'-\omega' t')}, \quad \textbf{(35)}$$

where $\beta'(\omega')$ is a dispersion relation of the core guided mode of a PC waveguide in the moving reference frame S' in which the waveguide is stationary (see Fig. 10, for example). Also according to the Bloch theorem, $\beta'(\omega')$ is confined to the first Brillouin zone $(-\pi/a, \pi/a]$, and $U'_{\pm\beta'(\omega')}(x',y')$ are the periodic functions along the x'-axis with a periodicity of a:

$$U'_{\pm\beta'(\omega')}(x'+a,y') = U'_{\pm\beta'(\omega')}(x',y'). \quad \textbf{(36)}$$

Applying LT to the phase component in Eq. (35) the electric field of the guided mode in the free space of a hollow core in the frame S could be expressed as

$$\boldsymbol{E}^*(x,y,t) \propto \hat{\boldsymbol{z}} \cdot U'_{\pm\beta'(\omega')}(\gamma(x-vt),y) \cdot e^{i[\pm\beta'(\omega')\cdot\gamma(x-vt)-\omega'\gamma(t-x\frac{v}{c^2})]}. \quad \textbf{(37)}$$

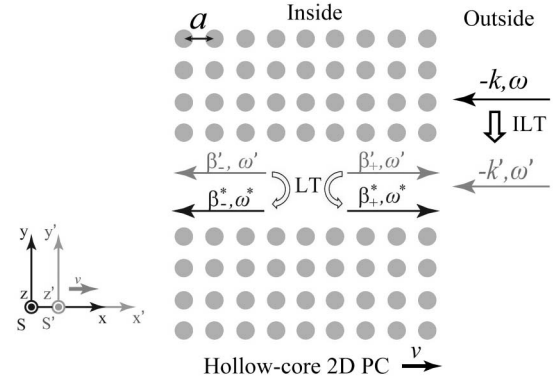

Fig. 9. Schematic of the excitation of guided modes in a moving hollow-core 2D PC waveguide.

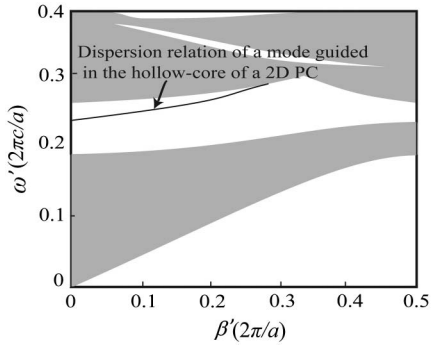

Fig. 10. Example of a dispersion relation of a core-guided mode of a hollow-core 2D PC waveguide (solid thick line). The gray regions represent continuum of the delocalized states inside of a 2D PC reflector (see page 154 in [1]). The PC reflector comprises a square lattice of rods suspended in air. The period of a square lattice is a. An individual rod has a dielectric constant $\epsilon_a = 9$ and a radius $r_a = 0.38a$. The hollow core is a defect introduced into a perfect PC lattice by removing one row of the dielectric rods.

As in the prior sections, we do not show explicitly the terms proportional to the magnetic field [see discussion after Eq. (19)]. Using discrete Fourier series for the periodic functions $U_{\pm\beta'(\omega')}(\gamma(x - vt), y)$, we have

$$U'_{\pm\beta'(\omega')}(\gamma(x - vt), y) = \sum_{n=-\infty}^{+\infty} A^n_{\pm\beta'(\omega')}(y) e^{i\frac{2\pi n}{a}\gamma(x-vt)}, \quad (38)$$

where n is an integer, and $A^n_{\pm\beta'(\omega')}$ are the Fourier coefficients. Substituting Eq. (38) into Eq. (37), we obtain the angular frequencies and the propagation constants of the guided modes inside of the moving 2D PC in the frame S:

$$\omega^*_{\pm,n} = \omega'\gamma \pm \beta'(\omega')v\gamma + \frac{2\pi v n\gamma}{a},$$
$$\beta^*_{\pm,n}(\omega) = \pm\beta'(\omega')\gamma + \frac{\omega' v\gamma}{c^2} + \frac{2\pi n\gamma}{a},$$
$$\omega' = \omega\gamma\left(1 + \frac{v}{c}\right). \quad (39)$$

We therefore conclude that two frequency combs are generated inside of the hollow core of a moving 2D PC that can be detected with a stationary detector placed in the waveguide hollow core.

In the limit of a large hollow core (by removing several rows of dielectric columns) the mode propagating in the free space of a hollow core has a modal effective refractive index close to that of the free space $n_{\text{eff}} \sim 1$. In this case, the modal dispersion relation $\omega'(\beta')$ within the fundamental bandgap can be simply approximated as

$$\omega'(\beta') = \beta' c, \qquad \beta' \in \left[0, \frac{\pi}{a}\right]. \quad (40)$$

Substituting Eq. (40) into Eq. (39), we get

$$\omega^*_{\pm n} = c\gamma\beta'\left(1 \pm \frac{v}{c}\right) + \frac{2\pi v n\gamma}{a},$$
$$\beta^*_{\pm n}(\omega) = \pm\gamma\beta'\left(1 \pm \frac{v}{c}\right) + \frac{2\pi n\gamma}{a}, \quad (41)$$

which can be further simplified to give

$$\omega^*_{\pm n} = \pm c\left(\beta^*_{\pm n} - \frac{2\pi n\gamma}{a}\left(1 \mp \frac{v}{c}\right)\right). \quad (42)$$

Using Eqs. (40)–(42), in Fig. 11 we plot dispersion relations of the two counterpropagating modes guided in a large hollow core of a moving 2D PC in the stationary frame S. We note that instead of plotting directly Eqs. (40)–(42) and having negative frequencies, we rather plot $sign(\omega^*) \cdot \omega^*$ and $sign(\omega^*) \cdot \beta^*(\omega^*)$. This way, only positive frequencies appear in the band diagrams, while the direction of wave propagation can still be referred from the sign of the propagation constant $sign(\omega^*) \cdot \beta^*(\omega^*)$. This follows from the observation that both $e^{i(\beta x - \omega t)}$ and $e^{i(-\beta x + \omega t)}$ define modes propagating in exactly the same direction.

5. COMPARISON OF DIFFERENT MOVING PC SYSTEMS AND DISCUSSION OF FACTORS RELATED TO THEIR EXPERIMENTAL FEASIBILITY

In this paper we have theoretically proposed several systems based on moving PCs for generation of new frequencies. We now summarize the properties of these systems and discuss their experimental feasibility. First, we considered reflection of monochromatic light by a semi-infinite 1D multilayer PC, assuming normal incidence of light onto a PC plane. In this case, the reflected wave shows a classic Doppler frequency shift ($\sim\frac{v}{c}$), similarly to the case of reflection form a single moving dielectric interface. In order to achieve maximum reflectivity, frequency of the incident light should be located within the PC bandgap as calculated in the moving reference frame S'. Next, we considered diffraction of a monochromatic light by a moving 1D grating (or a 1D PC in the transverse orientation). In this case we found [see Eq. (17)] that the frequencies, propagation directions, and amplitudes of the diffracted orders are similar, while somewhat different (by a factor of $\sim\frac{v}{c}$) from those of the diffraction orders generated by a stationary grating. After that we have analyzed generation of harmonics via excitation of the leaky waves of a moving 1D PC. In this case a finite PC (in the transverse direction) is excited with a monochromatic light that is incident normally onto the PC plane. Harmonics are then observed from the side by placing a detector outside of a PC. The frequency spacing of the generated harmonics could be calculated from Eq. (25) as $\Delta\omega^*_{\pm,n} = \frac{2\pi c}{a}\frac{v}{c}\gamma$, where a is a period of a photonic crystal in the moving reference frame S'. Thus, in order to simplify detection of such harmonics one interesting question is about increasing spacing between them. This can be achieved either by increasing the moving speed of a PC or decreasing the PC period a. As far as the first option is concerned, under regular laboratory conditions, $\frac{v}{c} \sim 10^{-5}$–10^{-6}. To pursue higher moving speed of PCs, one might consider immobilizing a PC on a projectile or satellite that travels with speeds of the order of

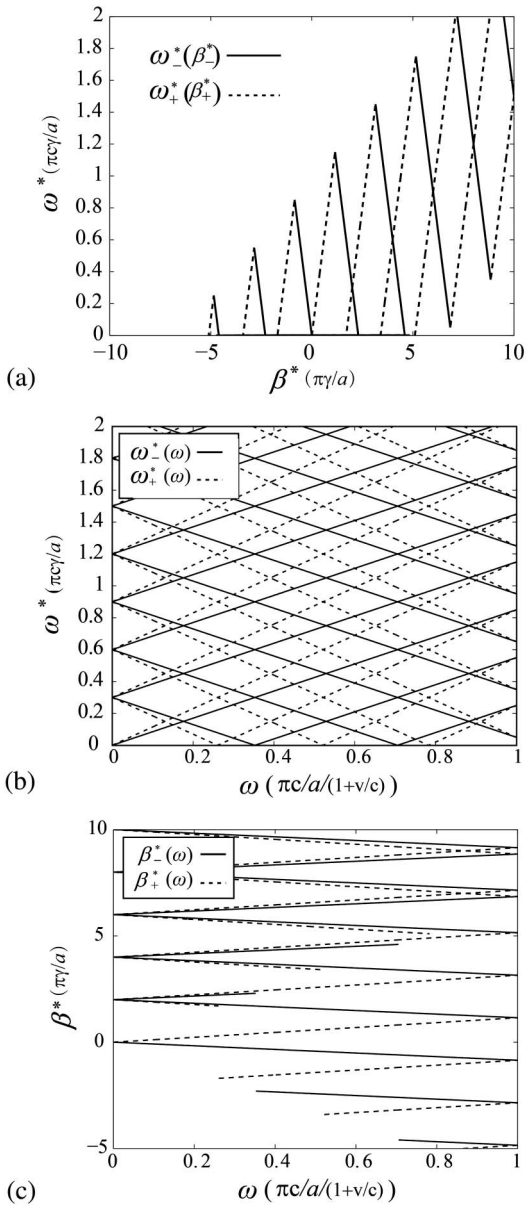

Fig. 11. (a) Dispersion relations (in the stationary frame S) of the two counterpropagating modes guided inside of a large hollow core of a moving 2D PC waveguide. The mode propagating along the x direction is shown as solid lines, while the mode propagating along $-x$ direction is shown as dashed lines. Here we use $v/c = 0.15$ in order to visually detect in the graphs above a pronounced shift in the frequency $\omega^*_{\pm n}$ in response to different harmonics orders. (b)–(c) Same two dispersion relations, however, now as a function of the excitation frequency ω. Clearly, for any given excitation frequency ω, there are two frequency combs $\omega^*_{\pm n}$ that are generated inside of a hollow core of a photonic crystal waveguide.

several kilometers/second. Another way to increase harmonics spacing is by decreasing the PC period a, while conserving its bandgap center wavelength λ'_c [note that λ'_c is the bandgap center wavelength; however, as shown in Fig. 5, the operation wavelength λ' in Eq. (18) should be slightly different from λ'_c, as λ' is chosen at the edge of the bandgap]. In the case of the normal incidence, PC geometrical parameters, such as low and high refractive index layer thicknesses are chosen using the quarter-wave condition $n_h d_h = \frac{\lambda'_c}{4}$, $n_l d_l = \frac{\lambda'_c}{4}$. As the PC period is $a = d_l + d_h = \frac{\lambda'_c}{4}(n_h^{-1} + n_l^{-1})$; therefore, its value could be minimized by using dielectric materials with relatively high refractive indices $n_{h,l} \gg 1$. Moreover, as mentioned in Section 4.B, amplitude of the generated harmonics associated with the leaky modes of moving PCs could be associated with the Fourier coefficients [Eq. (20)] of the modal field distributions. In a typical scenario when layer thicknesses inside of a PC multilayer have comparable dimension $d_l \sim d_h \sim a$, most of the energy in the generated harmonics will concentrate in the first few low-order harmonics. Consequently, detection of higher-order harmonics could be practically challenging. This can be alleviated by using coupled photonic crystal resonator arrays in which modal size in the resonance (resonator size d) can be much smaller than the distance between the individual resonators (period of the photonic crystal array a), thus allowing efficient excitation of the higher-order harmonics of up to $\sim\frac{a}{d}$. Finally, in our work we considered light guidance by a moving hollow-core Bragg waveguide as well as a hollow-core 2D PC. Of particular interest for practical implementation is a case of the hollow-core 2D PC, in which two frequency combs can be generated and potentially detected inside of the waveguide hollow core. As in the case of leaky modes of a finite-size PC, in order to simplify detection of the generated frequencies we need to increase spacing between the individual harmonics, as well as increase harmonic amplitudes. In order to increase harmonics spacing one has can either use high moving speed of the PC, or one can increase the ratio of the operational wavelength to the PC period $\frac{\lambda'}{a}$, which can be accomplished by using high refracting materials. Finally, in passing we mention that relative amplitudes of the higher-order harmonics can be enhanced by resorting to the coupled photonic crystal resonator arrays, while further studies are needed to fully elaborate the validity of this approach.

6. CONCLUSION

We have discussed the experimental feasibility and presented several system designs for the detection of new frequencies generated when light is interacting with the moving photonic crystals. We first presented a rigorous mathematical formulation for the analysis of reflection of an electromagnetic wave by a single moving dielectric interface. Next we have demonstrated that reflection from an infinite 1D PC (incidence direction is perpendicular to the multilayer plane) only results in a classic Doppler shift of the reflected light frequency, and in this respect it is similar to the reflection from a moving single dielectric interface. We have then described generation of frequency harmonics when incident light is diffracted by a moving diffractive grating or a 1D PC in the transverse orientation (incidence direction is parallel to the multilayers). Next we have described frequency harmonics generation via excitation of the leaky waves of a moving 1D PC. In this case, incidence direction is perpendicular to the multilayer plane; however, the PC is assumed to be of finite size in the transverse direction and new frequencies are observed at the PC edge. Finally, we have derived dispersion relations for the modes guided in the hollow

core of the moving hollow-core waveguides. In particular, we have concluded that in the case of the hollow-core 2D PC waveguides, two frequency combs are generated inside of the waveguide hollow core.

APPENDIX A

In Section 3, we mention that Maxwell's field equations are invariant under Lorentz transformation. In particular, the electric and magnetic fields in the free space in the stationary frame S are related to those in the moving frame S' as follows:

$$\boldsymbol{E}' = \gamma \boldsymbol{E} + (1-\gamma)\cdot(\boldsymbol{E}\cdot\boldsymbol{v})\frac{\boldsymbol{v}}{v^2} + \gamma(\boldsymbol{v}\times\boldsymbol{B}), \tag{A1}$$

$$\boldsymbol{B}' = \gamma \boldsymbol{B} + (1-\gamma)\cdot(\boldsymbol{B}\cdot\boldsymbol{v})\frac{\boldsymbol{v}}{v^2} - \frac{\gamma(\boldsymbol{v}\times\boldsymbol{E})}{c^2}. \tag{A2}$$

In the case of a plane wave with its electric field polarized in the z direction, and assuming the moving frame displacement in the x direction, Eqs. (A1) and (A2) could be simplified as

$$\boldsymbol{E}' = \gamma \boldsymbol{E} + \gamma(\boldsymbol{v}\times\boldsymbol{B}), \tag{A3}$$

$$\boldsymbol{B}' = \gamma \boldsymbol{B} - \frac{\gamma(\boldsymbol{v}\times\boldsymbol{E})}{c^2}. \tag{A4}$$

In addition, from the Maxwell equations, the electric and magnetic fields of a plane wave in the free space in the frame S are related as

$$\boldsymbol{E} = -\frac{\boldsymbol{k}\times\boldsymbol{B}}{\omega}\cdot c^2, \tag{A5}$$

$$\boldsymbol{B} = \frac{\boldsymbol{k}\times\boldsymbol{E}}{\omega}. \tag{A6}$$

Substituting Eqs. (A5) and (A6) into Eqs. (A3) and (A4), respectively, we get for the case of a plane wave:

$$\boldsymbol{E}' = \gamma \boldsymbol{E} + \frac{\gamma\boldsymbol{v}\times(\boldsymbol{k}\times\boldsymbol{E})}{\omega} = \gamma\boldsymbol{E}\left(1-\frac{v}{c}\right), \tag{A7}$$

$$\boldsymbol{B}' = \gamma \boldsymbol{B} + \frac{\gamma\boldsymbol{v}\times(\boldsymbol{k}\times\boldsymbol{B})}{\omega} = \gamma\boldsymbol{B}\left(1-\frac{v}{c}\right). \tag{A8}$$

Therefore, we conclude that when a plane wave is transformed from the stationary frame S into the moving frame S', the amplitudes of its electric and magnetic fields decrease by the factor $\gamma(1-\frac{v}{c})$.

Funding. Canada Research Chairs.

Acknowledgment. The funding for this research partially comes from the Canada Research Chairs Program.

REFERENCES

1. M. Skorobogatiy and J. Yang, *Fundamentals of Photonic Crystal Guiding* (Cambridge University, 2009).
2. J. D. Joannopoulos, S. G. Johnson, J. N. Winn, and R. D. Meade, *Photonic Crystals: Molding the Flow of Light* (Princeton University, 2011).
3. C. M. Soukoulis, *Photonic Crystals and Light Localization in the 21st Century* (Springer Science & Business Media, 2012).
4. Y. Xu and B. Chen, "Applications of photonic crystals in medicine," Clin. Lab. **61**, 11–16 (2014).
5. F. Begum and Y. Namihira, *Photonic Crystal Fiber for Medical Applications* (INTECH Open Access, 2012).
6. M. Grimann and T. Fuhrmann-Lieker, "Biological photonic crystals," in *Organic and Hybrid Photonic Crystals* (Springer, 2015), pp. 57–74.
7. L. Rindorf, J. B. Jensen, M. Dufva, L. H. Pedersen, P. E. Høiby, and O. Bang, "Photonic crystal fiber long-period gratings for biochemical sensing," Opt. Express **14**, 8224–8231 (2006).
8. K. P. Hansen, J. R. Folkenberg, A. Petersson, and A. O. Bjarklev, "Properties of nonlinear photonic crystal fibers for telecommunication applications," in *Optical Fiber Communication Conference* (Optical Society of America, 2003), paper FI2.
9. B. Gauvreau, N. Guo, K. Schicker, K. Stoeffler, F. Boismenu, A. Ajji, R. Wingfield, C. Dubois, and M. Skorobogatiy, "Color-changing and color-tunable photonic bandgap fiber textiles," Opt. Express **16**, 15677–15693 (2008).
10. B. Gauvreau, K. Schicker, N. Guo, C. Dubois, R. Wingfield, and M. Skorobogatiy, "Color-on-demand photonic textiles," Text. J. **125**, 70–81 (2008).
11. M. Skorobogatiy and J. Joannopoulos, "Photon modes in photonic crystals undergoing rigid vibrations and rotations," Phys. Rev. B **61**, 15554–15557 (2000).
12. M. Skorobogatiy and J. Joannopoulos, "Rigid vibrations of a photonic crystal and induced interband transitions," Phys. Rev. B **61**, 5293–5302 (2000).
13. K. R. Khan, T. X. Wu, D. N. Christodoulides, and G. I. Stegeman, "Soliton switching and multi-frequency generation in a nonlinear photonic crystal fiber coupler," Opt. Express **16**, 9417–9428 (2008).
14. A. Husakou and J. Herrmann, "Frequency comb generation by four-wave mixing in a multicore photonic crystal fiber," Appl. Phys. Lett. **83**, 3867–3869 (2003).
15. V. G. Veselago, "The electrodynamics of substances with simultaneously negative values of ϵ and μ," Phys. Usp. **10**, 509–514 (1968).
16. J. Chen, Y. Wang, B. Jia, T. Geng, X. Li, L. Feng, W. Qian, B. Liang, X. Zhang, and M. Gu, "Observation of the inverse Doppler effect in negative-index materials at optical frequencies," Nat. Photonics **5**, 239–245 (2011).
17. C. Luo, M. Ibanescu, E. J. Reed, S. G. Johnson, and J. Joannopoulos, "Doppler radiation emitted by an oscillating dipole moving inside a photonic band-gap crystal," Phys. Rev. Lett. **96**, 043903 (2006).
18. E. J. Reed, "Physical optics: Backwards Doppler shifts," Nat. Photonics **5**, 199–200 (2011).
19. D.-W. Wang, H.-T. Zhou, M.-J. Guo, J.-X. Zhang, J. Evers, and S.-Y. Zhu, "Optical diode made from a moving photonic crystal," Phys. Rev. Lett. **110**, 093901 (2013).
20. N. Hamdan, "On the invariance of Maxwell's field equations under Lorentz transformations," Galilean Electrodyn. **17**, 115–117 (2006).
21. C. A. Palmer, E. G. Loewen, and R. Thermo, *Diffraction Grating Handbook* (Newport Corporation, 2005).